Hindawi
Mathematical Problems in Engineering
Volume 2020, Article ID 1274728, 9 pages
https://doi.org/10.1155/2020/1274728

Research Article

Correction Method for Hydraulic Conductivity Measurements Made Using a Fixed Wall Permeameter

Qiang Luo,[1,2] Mengshi Liu,[2,3] Tengfei Wang ,[1,2] and Peng Wu[2,3]

[1]*MOE Key Laboratory of High-Speed Railway Engineering, Southwest Jiaotong University, Chengdu 610031, China*
[2]*School of Civil Engineering, Southwest Jiaotong University, Chengdu 610031, China*
[3]*China Railway Eryuan Engineering Group Co. Ltd., Chengdu 610031, China*

Correspondence should be addressed to Tengfei Wang; w@swjtu.edu.cn

Received 16 August 2019; Revised 5 November 2019; Accepted 21 December 2019; Published 13 January 2020

Academic Editor: Samuele De Bartolo

Hydraulic conductivity measurement through a fixed wall permeameter is a common practice to obtain the fluid transmissibility characteristics of soil matrix; however, sidewall leakage due to rigid wall effect may significantly influence the observed values for coarse-grained soils. In this study, the boundary flow error was identified through characterizing the geometrical properties of voids adjacent to the sidewall, and a parameter known as the boundary void ratio (e_b) was proposed to account for this effect. The findings suggest that a fixed wall cell containing coarse soils would unavoidably generate extra voids at the interface between soil grains and inner rigid wall, contributing to a larger e_b at the wall than void ratio within the soil bed; the measured hydraulic conductivity is increased primarily due to the apparatus-induced error. A two-dimensional geometric model was then established to estimate the e_b value for uniformly sized coarse soils confined by a rigid permeameter wall, based on which a method was obtained for eliminating the boundary flow error from a fixed wall cell. The mathematical method was finally validated against experimental data from existing literature. It can be concluded that the boundary condition at sidewall featuring unwanted gaps lead to overestimation of the coefficient of permeability; however, the proposed correction method could adequately eliminate the boundary flow error for uniformly sized coarse-grained soils tested within a rigid wall cell.

1. Introduction

Soil mass made up of solid particles with necessary voids can allow water to pass through [1, 2]. Hydraulic conductivity (also referred to as the permeability coefficient) defined by Darcy's law is an essential parameter for identifying the permeability of soils under the laminar flow region. Currently, there are two typical types of permeameter used for measuring the hydraulic conductivity in the laboratory, namely, fixed wall permeameter [3] and flexible-wall permeameter [4]. Fixed wall cell mainly consists of a rigid cylindrical tube and offers the benefits, such as simplicity, low cost, and the convenience for specimen preparation. At the same time, the shortcoming is obvious since the wall effect for particles packing adjacent to the wall might lead to potential sidewall leakage and flow maldistribution and an exaggerated permeability of laboratory test as well; i.e., the hydraulic conductivity value for finite bed is greater than that for infinite bed [5, 6]. A flexible-wall device comprises a triaxial cell, in which the bed is enclosed by a flexible membrane and subjected to controlled confining pressure. It can effectively eliminate boundary flow issue, and the measured data are close to the real hydraulic conductivity of unconfined bed. Thus, more researchers were focused on employing flexible-wall permeameter for hydraulic conductivity measurements [7–9]. However, complicated operations and high cost set limits for a widespread use [10].

Concerning a fixed wall cell, the boundary effect has long been investigated. Franzini [11] demonstrated that the porosity in the vicinity of sidewall is greater than within the bed packed with grains because the grains close to the wall cannot be packed as tightly as those inside soil bed. The bed can be divided into two zones, namely, the outer shell near the wall and the core whose porosity is free from the boundary effect.

Meanwhile, Roblee et al. [12] and Ridgway and Tarbuck [13] conducted several elaborate measurements of the porosity on uniformly sized grains contained in a rigid cylindrical tube, through pouring the wax into the bed to fix them in position. By analyzing variation law of porosity with the distance away from sidewall, Cohen and Metzner [14] suggested using a triregional model to partition the cross section of confined bed, namely, a wall region, a transition region, and a bulk region, each with a different porosity. Moreover, based on the capillary model from Carman [15], the flow distribution in each region was considered, and they concluded that the boundary influence on water flow could be ignored when the ratio of tube diameter to grains diameter is greater than approximately 30 for Newtonian fluids and 50 for non-Newtonian fluids. de Klerk [16] established a mathematical model with an exponential decay function for describing the porosity variation in the radial direction and predicted the average porosity of confined bed.

More recently, Allen et al. [17], Yadav [18], and Larsson et al. [19] reached an agreement on the effect of permeameter boundary on water flow primarily displayed in two contradictory aspects: (1) the increased porosity near the wall would reduce the resistance to flow; therefore, sidewall leakage occurs; (2) the presence of shearing stress due to a larger surface area at the wall increases flow resistance, inducing reduction in hydraulic conductivity of confined bed. Kango et al. [20] carried out a series of permeability tests for natural soils with different permeameters to particle size ratios (i.e., D_p/d_g, where D_p is the permeameter diameter and d_g is the particle diameter) and found that the influence of increasing porosity is more pronounced than surface are at the wall for $D_p/d_g < 40$, and thus the hydraulic conductivity of confined bed (k) would be greater than unconfined conditions (k^*). However, there would be a reversal phenomenon for D_p/d_g ranging between 40 and 120, and the wall effect is negligible provided that $D_p/d_g > 120$.

In summary, small-scale fixed wall permeameter does not require excessive soil samples and high water flow from permeability apparatus that make it difficult to conduct in the laboratory [21]. However, the related boundary flow issue in a permeability test shall be carefully dealt with. In this paper, the underlying mechanism of the wall effect was firstly elucidated by analyzing boundary void characteristics in the confined bed. Second, within the 2D theoretical framework, a geometric model was proposed to estimate the boundary void ratio of coarse-grained soils adjacent to the wall. Finally, based on the relationship between void ratio and hydraulic conductivity, a correction method was developed for hydraulic conductivity measured in a fixed wall cell and verified against test data from the existing literature. It should be emphasized that this is only a simplistic approach for uniformly sized coarse-grained soils. Further investigation is required to extend its application to soils having different grain dimensions.

2. Boundary Void Characterization

Several techniques (SEM, MIP, and X-ray computed microtomography) have been developed to reveal the inner structure of compacted soils. There are not only intraparticle voids but also interparticles, and the voids present a wide range of dimensions, varying with different conditions such as loading and compaction [22]. They jointly contribute to the real complexity of the inner structure, which cannot be fully accounted for in this study. Some simplifications have been made before characterizing boundary voids of coarse-grained soils. Figure 1 shows a plane view of composition characteristics of voids near the sidewall within a fixed wall cell, where soil voids are of two general types: typical void among the matrix particles, V_0, and boundary void adjacent to rigid wall, V_b. In order to further distinguish V_0 and V_b, a few hypothetical matrix particles, which have the same packing characteristics as the existing matrix particles, are assigned along with the boundary voids, as specified in Figure 1. Thus, V_b consists of two parts: V_v refers to the volume of voids encircled by the hypothetical matrix particle and existing matrix particles next to it, equaling to V_0; V_p denotes the overlap fraction of the hypothetical matrix particle plus V_b.

As demonstrated in Figure 1, it is also reasonable to assume that V_v consists of V_1 and V_2, where V_1 represents the volume associated with the existing matrix particles surrounding V_v and V_2 refers to a volume formed by the hypothetical matrix particle next to it. This implies that some extra voids would exist around the surface of the wall when compared to those in the interior of the bed since the soil solids are not essentially contacting the rigid wall. The extra void (i.e., V_f) caused by sidewall can be expressed as follows:

$$V_f = V_b - V_1 = V_p + V_2. \tag{1}$$

As shown in Figure 1, V_2 in equation (1) is associated with the grain size as well as the compaction level of the bed and is independent of permeameter diameter. V_p in equation (1), however, is connected to all the factors mentioned above. Besides, a larger permeameter diameter D leads to a smaller volume of hypothetical matrix particle that is placed next to boundary particles, as well as a reduction in V_p.

Hence, it can be concluded that V_b can also be treated as the sum of V_1 and V_f, which are related to the existing matrix particles surrounding V_b and the permeameter wall, respectively. Referring to the definition of void ratio from soil mechanics, boundary void ratio (BVR, e_b) at the inner wall for confined bed can be accordingly defined as follows:

$$e_b = \frac{V_b}{V_s} = \frac{V_1 + V_f}{V_s} = e + \frac{V_f}{V_s}, \tag{2}$$

where V_s is the partial volume of the existing matrix particles near the wall, which contributes to the void V_1 (i.e., the shaded area in Figure 1) and e denotes the void ratio of the soil bed.

The presence of extra void, V_f, would produce a larger e_b than e, increase the seepage velocity in the vicinity of wall, and ultimately induce sidewall leakage. It should be noted that the measured hydraulic conductivity would be overestimated when V_f is ignored.

3. Mathematical Formulation

Figure 2 illustrates an overview of uniformly sized disks packing in a 2D problem. The regular triangle packing

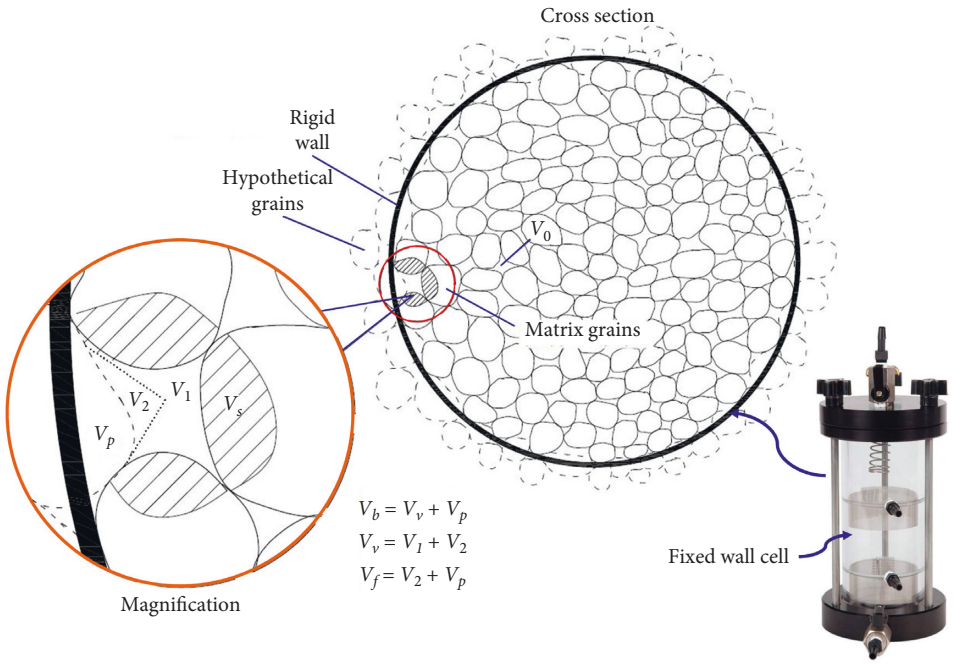

Figure 1: Schematic of plane distribution of soil voids adjacent to rigid wall.

(Figure 2(a)) and the square packing (Figure 2(c)) can produce the densest and loosest states, respectively. Therefore, the density of other rhombus packing falls within this range (Figure 2(b)). By connecting the centers of adjacent four disks, e.g., $o_1o_2o_3o_4$ in Figure 2, and defining the packing angle as $\angle o_2o_1o_3 = \alpha(\pi/3 \le \alpha \le \pi/2)$, the plane void ratio (PVR) e' can be expressed as follows:

$$e' = \frac{4\sin\alpha}{\pi} - 1. \tag{3}$$

As α increases, the void size in a packing unit $o_1o_2o_3o_4$ and $e\prime$ would monotonously increase, leading to a reduction in density. In particular, if α equals to $\pi/3$ or $\pi/2$, the minimum $e'_{\min} = 0.103$ and the maximum $e'_{\max} = 0.273$ can be thus obtained, respectively [23].

Owing to numerous factors affecting the boundary void, some necessary simplifications are made before establishing a theoretical model. In this paper, the soil mass in a permeameter cell are assumed to be composed of uniform circular disks in a plane with packing angle α as an indication of packing density. Through replacing partial disks of a packing unit $o_1o_2o_3o_4$ with the permeameter wall, a simplified geometric model is developed to estimate e_b, as shown in Figure 3.

In this model, the inner wall of permeameter has a radius of $D/2$, and the disks having a uniform diameter of d next to the wall represent the soil particles. Moreover, the blank area between the wall and the particles refers to the boundary void V_b, around which are two tangent points between the wall and the particles. Within the framework of the computational model, a disk refers to soil particle, while the gap between the wall and the particles represents the boundary void. The thickness of sidewall has thus been ignored.

In the packing unit $o_1o_2o_3o_4$ where $\pi/3 < \alpha \le \pi/2$, three boundary-packing types are clarified for V_b, with multiple disks removed and replaced by the wall. Thereafter, the plane boundary void ratio (PBVR, e'_b) is proposed, which can be determined for certain boundary-packing types.

Type I: V_b is surrounded by any two tangent particles of unit $o_1o_2o_3o_4$ and permeameter wall. For instance, as shown in Figure 3(a), o_3 and o_4 are assumed to be replaced by the wall; Hence, the wall is tangent to the particles o_1 and o_2, and the corresponding θ_1 can be calculated as

$$\theta_1 = 2\arcsin\frac{d}{D-d}. \tag{4}$$

The area $A_1B_1C_1$ excluding disks in Figure 3(a) represents V_b, which can be easily inferred:

$$S_{A1B1C1} = \frac{\theta_1}{8}(D-d)(D+d) - \frac{d}{4}(D-d)\cos\frac{\theta_1}{2} - \frac{\pi d^2}{8}. \tag{5}$$

A complete void for unit $o_1o_2o_3o_4$ corresponds to an area of an individual particle. V_b is surrounded by two particles in Figure 3(a), based on the adjacent complementation law of the interior angles for rhombus, and the disk V_s corresponding to void V_1 in Figure 1 shall be

$$S_{s1} = \frac{1}{2}\times\frac{\pi d^2}{4} = \frac{\pi d^2}{8}. \tag{6}$$

Combining Equations (2), (5), and (6), the PBVR e'_{b1} for Type I can be obtained as follows:

$$e'_{b1} = \frac{S_{A1B1C1}}{S_{s1}} = \frac{2}{\pi d^2}(D-d)(D+d)\arcsin\frac{d}{D-d} - \frac{2}{\pi d}\sqrt{D^2-2Dd} - 1. \tag{7}$$

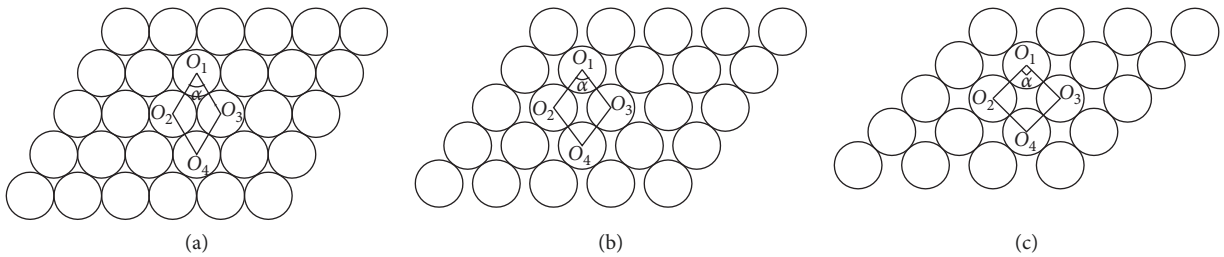

Figure 2: Uniformly sized disks packing in a plane: (a) $\alpha = \pi/3$; (b) $\pi/3 < \alpha < \pi/2$; (c) $\alpha = \pi/2$.

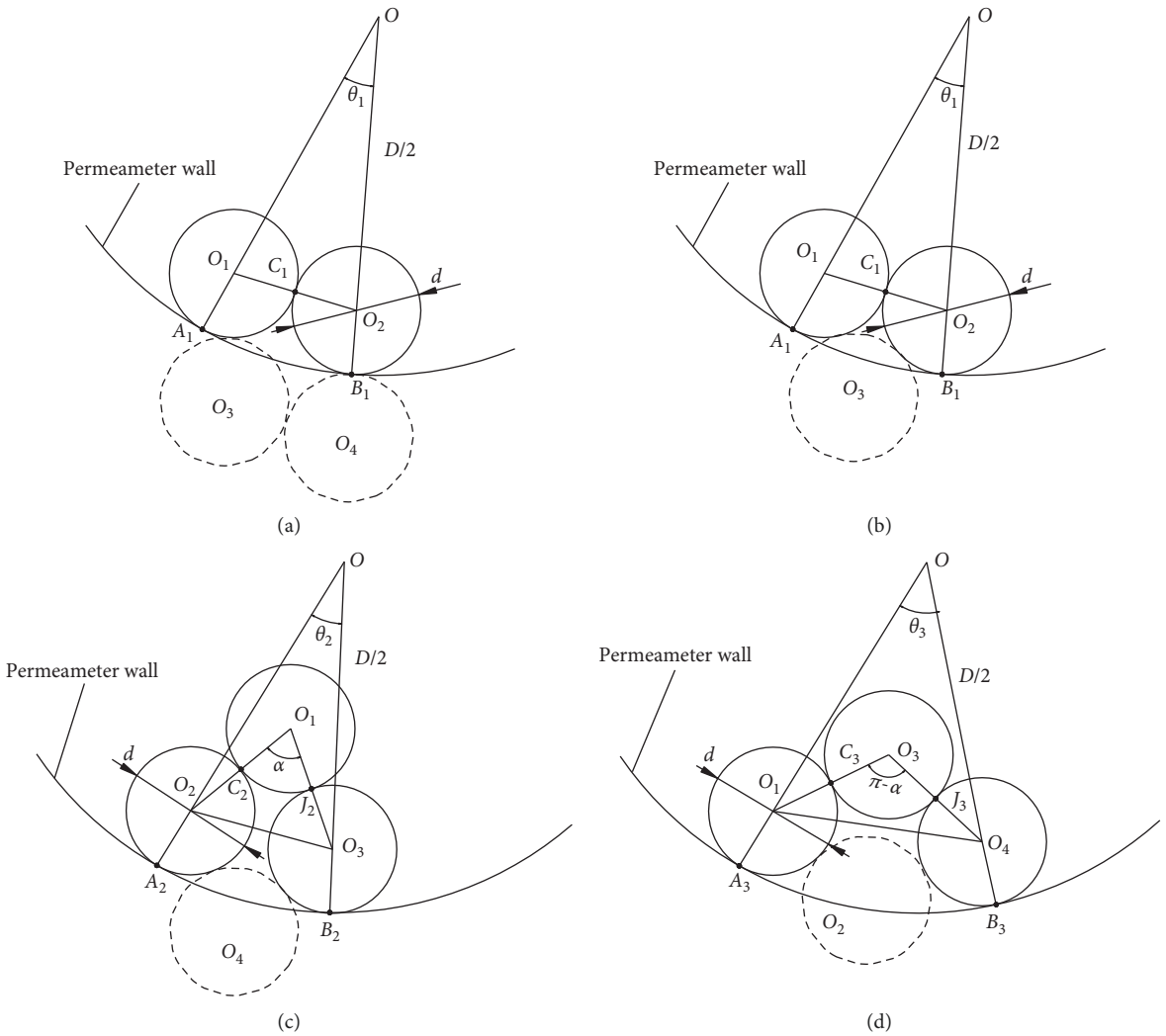

Figure 3: Computational model for 2D void ratio determination at sidewall: (a) Type I-1 ($\pi/3 < \alpha \leq \pi/2$); (b) Type I-2 ($\alpha = \pi/3$); (c) Type II ($\pi/3 < \alpha \leq \pi/2$); (d) Type III ($\pi/3 \leq \alpha \leq \pi/2$).

Type II: V_b is jointly surrounded by any three particles in unit $o_1o_2o_3o_4$ and permeameter wall. In addition, the lines connecting the centers of these particles generate a triangle (e.g., when $\alpha = \pi/2$, a right triangle will be). For instance, by replacing particle o_4 with the wall in Figure 3(c), θ_2 can be calculated by

$$\theta_2 = 2 \arcsin \frac{2d \sin(\alpha/2)}{D - d}. \tag{8}$$

Similarly, the area $A_2B_2C_2J_2$ standing for V_b equals to

$$S_{A2B2C2J2} = \frac{\theta_2}{8}(D-d)(D+d) + \frac{2\sin\alpha - \pi}{4}d^2 - \frac{1}{8}(D-d)^2\sin\theta_2. \tag{9}$$

As can be seen in Figures 2(b) and 3(c), the particle o_4 is replaced by a wall; therefore, the disk area S_{s2} representing V_s can be obtained:

$$S_{s2} = \left(1 - \frac{\alpha}{2\pi}\right)\frac{\pi d^2}{4}. \tag{10}$$

To sum up, the PBVR e'_{b2} for Type II is

$$e'_{b2} = \frac{S_{A2B2C2J2}}{S_{s2}} = \frac{1}{((2\pi-\alpha)d^2)/8}\left[\frac{2\sin\alpha-\pi}{4}d^2 + \frac{1}{4}(D-d)(D+d)\arcsin\frac{2d\sin(\alpha/2)}{D-d} - \frac{1}{8}(D-d)^2\sin\cdot\left(2\arcsin\frac{2d\sin(\alpha/2)}{D-d}\right)\right]. \tag{11}$$

Type III: V_b is jointly surrounded by any three particles of unit $o_1o_2o_3o_4$ and the permeameter wall. It should be noted that the lines connecting the centers of these particles create an obtuse triangle (when $\alpha = \pi/2$, it will then be a right triangle). If so, replacing particle o_2 with the wall in Figure 3(d), θ_3 will be expressed by

$$\theta_3 = 2\arcsin\frac{2d\sin((\pi-\alpha)/2)}{D-d}. \tag{12}$$

Following the same procedure for Type II, the area $A_3B_3C_3J_3$ representing V_b and the PBVR e'_{b3} for Type III are calculated as follows:

$$S_{A3B3C3J3} = \frac{\theta_3}{8}(D-d)(D+d) + \frac{2\sin(\pi-\alpha)-\pi}{4}d^2 - \frac{1}{8}(D-d)^2\sin\theta_3, \tag{13}$$

$$e'_{b3} = \frac{8}{(\pi+\alpha)d^2}\left[\frac{2\sin(\pi-\alpha)-\pi}{4}d^2 + \frac{1}{4}(D-d)(D+d)\cdot\arcsin\frac{2d\sin((\pi-\alpha)/2)}{D-d} - \frac{1}{8}(D-d)^2\sin\cdot\left(2\arcsin\frac{2d\sin((\pi-\alpha)/2)}{D-d}\right)\right]. \tag{14}$$

Among all the boundary-packing types mentioned above, it is apparent that PBVRs for Type I, Type II, and Type III are in the ascending order, primarily due to the increased representative area of V_b.

To be more specific, the particle o_2 contacts the particle O_3 when $\alpha = \pi/3$ (Figure 2(a)). More importantly, it also serves as a boundary between Type II and Type I in Figure 3. Hence, there are two general boundary-packing types for the particles adjacent to the wall, namely, Type I and Type III. As shown in Figure 2(a), it is three particles that surround a single pore of unit $o_1o_2o_3o_4$, so that a pore corresponds to half of a particular area that is different from Figures 2(b) and 2(c). Because the wall replaces one particle and combines the other two particles to form such a boundary void in Type I (Figure 3(b)), based on the sum of the interior angles of a triangle, the disk area of V_s is given as follows:

$$S_{s1,\alpha=\pi/3} = \frac{2}{3}\times\frac{\pi d^2}{8} = \frac{\pi d^2}{12}. \tag{15}$$

Substituting equations (5) and (15) into equation (2) yields

$$e'_{b1,\alpha=\pi/3} = \frac{3}{\pi d^2}\left[(D-d)(D+d)\arcsin\frac{d}{D-d} - d\sqrt{D^2-2Dd} - \frac{\pi d^2}{2}\right]. \tag{16}$$

Moreover, another boundary-packing type (i.e., Type III) is the same as that in Figure 3(d); then, PBVR $e'_{b3,\alpha=\pi/3}$ for Type III remains unchanged when compared to e'_{b3}, indicating that it can be calculated by equation (14).

On the premise of that α is a constant, with the various numbers and locations of particles within a certain unit $o_1o_2o_3o_4$ replaced by a sidewall, the number of combinations of the residual particles to form the boundary void should be 8 (referring to Table 1). Assuming that all the combinations follow the principle of random events, the probability of boundary-packing types, namely, P_1, P_2, and P_3 corresponding to Types I, II, and III, respectively, have been tabulated in Table 1, including such particular conditions as $\pi/3 < \alpha \le \pi/2$ and $\alpha = \pi/3$. When $\pi/3 < \alpha \le \pi/2$, there are four particle combinations for Type I-1, two for Type II, and two for Type III; when $\alpha = \pi/3$, there are six particles combinations in total for Type I-2 and just two for Type III.

4. Correction Method

As discussed above, if extra void contributing to potential sidewall leakage is known, the error of measured hydraulic conductivity through fixed wall permeameter can be corrected accordingly. Based on a plane-geometric model for calculating PBVR, the main computation procedure to correct the hydraulic conductivity of uniformly sized coarse-grained soils is given as follows.

Step 1. determining the average grain size of the material tested. The disks diameter (d) in the PBVR geometric model is regarded as the geometric-equivalent diameter of poorly graded coarse soils obtained from standard sieve analysis. The applicability of this correction method in well graded soils has not been fully discussed and illuminated.

Step 2. determining the correction factor for PBVR. Following the assumption that the uniform disks with $\alpha = \pi/3$, $\pi/2$ corresponds to the densest or the loosest state of the soil

Table 1: Probability summary of boundary-packing types in the PBVR geometric model.

Packing angle α	Boundary-packing type	Particle combination	Probability	PBVR
$\pi/3 < \alpha \le \pi/2$	Type I	O_1O_2, O_1O_3, O_2O_4, O_3O_4	$P_1 = 0.50$	Equation (7)
	Type II	$O_1O_2O_3$, $O_2O_3O_4$	$P_2 = 0.25$	Equation (11)
	Type III	$O_1O_2O_4$, $O_1O_3O_4$	$P_3 = 0.25$	Equation (14)
$\alpha = \pi/3$	Type I	O_1O_2, O_1O_3, O_3O_4, O_2O_4, $O_1O_2O_3$, $O_2O_3O_4$	$P_1 = 0.75$	Equation (16)
	Type II	N/A	$P_2 = 0$	N/A
	Type III	$O_1O_2O_4$, $O_1O_3O_4$	$P_3 = 0.25$	Equation (14)

sample, respectively. Thus, the soil bed in the permeameter with any given compaction level can be reproduced by the plane packing of uniform disks in Figure 2 with a specific packing angle α ranging from $\pi/3$ to $\pi/2$.

Since the soil particles are simplified as mono-sized 2D disks in the model development, it cannot fully reflect the real packing characteristics under 3D conditions, under the effect of grain shape, spatial dimension, and the variability between the overlapping 2D disks. Assuming that the compaction levels for the uniformly sized disks in a plane and compacted soil bed are controlled as the same, the difference between PVR (e') and the real void ratio should be accordingly modified, given by

$$e = \xi e', \tag{17}$$

where ξ is the correction factor for PVR.

For the densest scenario, the corresponding correction factor $\xi_{\min}$ is calculated through comparing $e'_{\min}$ to the minimum void ratio $e_{\min}$ as follows:

$$\xi_{\min} = \frac{e_{\min}}{e'_{\min}} = 9.71e_{\min}. \tag{18}$$

Likewise, the correction factor $\xi_{\max}$ for the loosest scenario shall be

$$\xi_{\max} = \frac{e_{\max}}{e'_{\max}} = 3.66e_{\max}, \tag{19}$$

where $e_{\max}$ denotes the maximum void ratio.

Therefore, the correction factor ξ for the confined bed with any given compaction level corresponding to the void ratio e could be obtained through linear interpolation between $\xi_{\min}$ and $\xi_{\max}$, and thus,

$$\begin{aligned}\xi = \xi_{\min} + \frac{(e - e_{\min})(\xi_{\max} - \xi_{\min})}{(e_{\max} - e_{\min})} = 9.71e_{\min} \\ + (3.66e_{\max} - 9.71e_{\min})\frac{e - e_{\min}}{e_{\max} - e_{\min}}.\end{aligned} \tag{20}$$

Step 3. determining the packing angle. It can be seen from equation (17) that e is dependent on e'. Also, e' is positively related to α in equation (3). Hence, in order to reflect the compaction level of the confined bed in plane whose void ratio is e, α for uniform disks packing in plane is expressed from equation (21) by considering equations (3) and (17):

$$\alpha = \arcsin\left[\frac{\pi}{4}\left(\frac{e}{\xi} + 1\right)\right]. \tag{21}$$

Step 4. calculating the area ratio of wall region and PBVR. Employing the measurement of water flow rate Q_t at the permeameter outlet and hydraulic gradient J across the test length of the soil bed for certain period, the observed value of hydraulic conductivity for confined bed in a fixed wall cell, i.e., k_t, could be obtained by Darcy's law:

$$k_t = \frac{Q_t}{A_t J}, \tag{22}$$

where A_t is the clearance cross-sectional area of permeameter, $A_t = \pi D^2/4$.

It is reasonable to assume that Q_t is divided into two parts, i.e., Q_c flows through the interior region of the bed and Q_w flows through the wall region, consistent with the assumption of [11]. If the water flow near the wall still obeys Darcy's law and has the same hydraulic gradient as the interior one, equation (22) can be transformed into

$$\begin{aligned}k_t = \frac{Q_c + Q_w}{A_t J} = \frac{k_c A_c J + k_w A_w J}{A_t J} = k_c\frac{A_c}{A_t} \\ + k_b\frac{A_w}{A_t} = k_c\left(1 - \frac{A_w}{A_t}\right) + k_w\frac{A_w}{A_t},\end{aligned} \tag{23}$$

where k_c is the hydraulic conductivity for the interior region, which equals to the hydraulic conductivity without confinement; k_w is the hydraulic conductivity for the wall region; and A_c and A_w represent the cross section areas of the interior region and the wall region, respectively. In addition, $A_w + A_c = A_t$.

As illustrated in equation (23), only when the area ratio of wall region λ (where $\lambda = A_w/A_t$) is small enough that it can be ignored. In other words, the interior region is much larger than the wall region; k_t would approximate the unconfined value, k_c. Owing to the empirical equation proposed by Liu [24, 25], which revealed a third-order nonlinear relationship between porosity and hydraulic conductivity of cohesionless soil shown in equation (24), a relationship between k_t and k_c thus is deduced in equation (25) by the combination of equations (23) and (24):

$$k = \beta n^3 = \beta\left(\frac{e}{1 + e}\right)^3, \tag{24}$$

where n is the porosity of soils and β refers to the coefficient for the influence of particle graduation.

$$k_t = \frac{k_c}{1 + \lambda\left[\left((e_b + e \cdot e_b)/(e + e \cdot e_b)\right)^3 - 1\right]}. \tag{25}$$

Table 2: Summary of corrected hydraulic conductivities against observed values for confined soil bed.

No.	D (mm)	d (mm)	E	e_{max}	e_{min}	ξ	α	e_b	λ	k_c (cm/s)	Test results [20]		Correction value	
											k_t (cm/s)	δ_1 (%)	k_t' (cm/s)	δ_2 (%)
1	50.8	4.00	0.590	0.786	0.372	3.225	1.192	1.688	0.181	7.28	11.60	59.3	6.83	6.2
2	50.8	2.80	0.572	0.786	0.372	3.256	1.177	1.635	0.129	4.00	5.68	42.0	3.76	6.0
3	50.8	1.70	0.565	0.786	0.372	3.269	1.171	1.585	0.079	1.82	2.37	30.2	1.81	0.5

Note: absolute relative error $\delta_1 = |k_t - k_c|/k_c$ and $\delta_2 = |k_t' - k_c|/k_c$.

According to the geometric model in a plane used for calculating PBVR, the area of the wall region in Type I, Type II, and Type III, namely, A_{w1}, A_{w2}, and A_{w3}, respectively, are inferred as follows:

$$A_{w1} = \left(1 + \frac{1}{e'_{b1}}\right) S_{A1B1C1},$$

$$A_{w2} = \left(1 + \frac{1}{e'_{b2}}\right) S_{A2B2C2J2}, \tag{26}$$

$$A_{w3} = \left(1 + \frac{1}{e'_{b3}}\right) S_{A3B3C3J3},$$

where e'_{b1}, e'_{b2}, and e'_{b3} can be calculated in Table 1; the expression of S_{A1B1C1}, $S_{A2B2C2J2}$, and $S_{A3B3C3J3}$ can be found from equations (5), (9), and (13), respectively.

Therefore, the area ratio of the wall region for three boundary-packing types (λ_1, λ_2, and λ_3) can be accordingly expressed as follows:

Type I:

$$\lambda_1 = \frac{A_{w1}}{S_{OA1B1}} = \frac{(1 + 1/e'_{b1}) S_{A1B1C1}}{S_{OA1B1}}. \tag{27}$$

Type II:

$$\lambda_2 = \frac{A_{w2}}{S_{OA2B2}} = \frac{(1 + 1/e'_{b2}) S_{A2B2C2J2}}{S_{OA2B2}}. \tag{28}$$

Type III:

$$\lambda_3 = \frac{A_{w3}}{S_{OA3B3}} = \frac{(1 + /1/e'_{b3}) S_{A3B3C3J3}}{S_{OA3B3}}, \tag{29}$$

where the section areas of S_{OA1B1}, S_{OA2B2}, and S_{OA3B3}, which denote A_t in Type I, Type II, and Type III, respectively, are obtained as follows:

$$S_{OAiBi} = \frac{D^2}{8}\theta_i, \quad (i = 1, 2, 3). \tag{30}$$

Hence, considering the probability of boundary-packing types, i.e., P_1, P_2, and P_3, in Table 1, e_b and λ can be expressed by

$$e_b = \xi \sum_{j=1}^{3} e'_{bj} P_j, \tag{31}$$

$$\lambda = \sum_{j=1}^{3} \lambda_j P_j. \tag{32}$$

Step 5. correcting hydraulic conductivity. Substituting equations (31) and (32) into equation (25) yields the correction value of hydraulic conductivity for confined bed:

$$k_t' = \frac{k_t}{\left\{1 + \lambda\left[\left((e_b + e \cdot e_b)/(e + e \cdot e_b)\right)^3 - 1\right]\right\}}. \tag{33}$$

To verify the rationality of the proposed correction method, the constant falling head experiments conducted by Kango et al. [20] in a fixed wall cell with uniformly sized soils (e.g., sand, marble chips, and gravels) were used as a reference. The collected data of hydraulic conductivities with $D/d < 40$ are demonstrated in Table 2 because the permeameter boundary predominates over other factors' influence on the permeability test results under such conditions. Unfortunately, since the values of e_{max} and e_{min} for these soil samples have not been provided in [20], the maximum and minimum void ratio of monodisperse sand in [26] shall be chosen to substitute them during the overall computational process, namely, $e_{max} = 0.786$ and $e_{min} = 0.372$. Additionally, k_c in Table 2 representing the hydraulic conductivity of unconfined bed is measured with D/d greater than 120, where the wall effect is not significant concerning the permeability test results and the permeameter wall could be assumed to be infinite as well [20, 27].

The k_t/k_c value was greater than the allowable error (i.e., 1.25) [3], indicating that the increase in k_t is mainly because of extra void V_f in Figure 1 and greater boundary void ratio e_b at the wall. After adopting the above procedures to revise these permeability test results, the correction values of hydraulic conductivity are also shown in Table 2. The ratio k_t'/kc approximates one, indicating that the corrected hydraulic conductivity of confined bed is consistent with that of unconfined bed in the proposed method.

Though the proposed method can correct hydraulic conductivity to some extent, the limitations of the model lie in that the soil particles in the confined bed are simplified as mono-sized 2D disks, which differs from the natural deposits. As a result, it is desirable to treat the soil particles as 3D balls to establish a computational model for boundary void ratio. Besides, this method can only be applied to uniformly sized soils. Given the real granulometric composition of naturally occurring soil that is composed by grains of various dimensions, further investigations need to be carried out to enhance the method's capability. It should also be noted that things become much more complex as more than two grain diameters are involved in developing a geometric model.

5. Conclusions

The boundary effect derived from fixed wall cell was investigated by analyzing the composition characteristics of voids close to sidewall, whereby the boundary void ratio (e_b) was defined for quantifying the wall effect within confined bed. It appears that the extra void adjacent to rigid wall should depend upon the grain size, compaction level of soil bed, and permeameter diameter. It should be noted that e_b is likely greater than the void ratio in the interior of the bed and contributes to the sidewall leakage during a permeameter test. Assuming that the soil particles of compacted bed are uniform disks packing in a plane, a geometric model for estimating e_b was established. Based on this model and employing an empirical relationship between void ratio and hydraulic conductivity, a correction method for the measured hydraulic conductivity using a fixed wall permeameter was proposed. The experimental data from published literature verified the feasibility of this method for uniformly sized coarse-grained soils. Further developments regarding the correction method should take gradation characteristics into account and derive a generalized formula. Notwithstanding such limitations, it can be treated as a promising step towards providing reliable references for the application of a fixed wall permeameter in laboratory tests.

Data Availability

The data used to support the findings of this study are available from the corresponding author upon request.

Conflicts of Interest

The authors declare that there are no conflicts of interest regarding the publication of this paper.

Acknowledgments

This work was supported by the National Natural Science Foundation of China (grant nos. 51878560 and 41901073) and China Postdoctoral Science Foundation (grant no. 2019M663556).

References

[1] K. Dolzyk and I. Chmielewska, "Predicting the coefficient of permeability of non-plastic soils," *Soil Mechanics and Foundation Engineering*, vol. 51, no. 5, pp. 213–218, 2014.

[2] B. Indraratan, V. T. Nguyen, and C. Rujikiatkamjorn, "Hydraulic conductivity of saturated granular soils determined using a constriction-based technique," *Canadian Geotechnical Journal*, vol. 49, no. 5, pp. 607–613, 2012.

[3] ASTM D5856-15, *Stand Test Method for Measurement of Hydraulic Conductivity of Porous Material Using a Rigid-Wall or Compaction-Mold Permeameter*, ASTM International, West Conshohocken, PA, USA, 2015.

[4] ASTM D5084-03, *Standard Test Methods for Measurement of Hydraulic Conductivity of Saturated Porous Materials Using a Flexible Wall Permeameter*, ASTM International, West Conshohocken, PA, USA, 2004.

[5] R. P. Chapuis, "Permeability tests in rigid-wall permeameters: determining the degree of saturation, its evolution, and its influence on test results," *Geotechnical Testing Journal*, vol. 27, no. 3, p. 10905, 2004.

[6] L. David Suits, T. C. Sheahan, A. T. Yeung, and S. M. Sadek, "Apparatus induced error in hydraulic conductivity measurement using a Lucite® fixed wall permeameter," *Geotechnical Testing Journal*, vol. 28, no. 5, p. 12527, 2005.

[7] C. H. Benson and N. Yesiller, "Variability of saturated hydraulic conductivity measurements made using a flexible-wall permeameter," *Geotechnical Testing Journal*, vol. 39, no. 3, Article ID 20150138, 2016.

[8] A. S. Samingan, E. C. Leong, and H. Rahardjo, "A flexible wall permeameter for measurements of water and air coefficients of permeability of residual soils," *Canadian Geotechnical Journal*, vol. 40, no. 3, pp. 559–574, 2003.

[9] X. Wang and C. H. Benson, "Constant-head constant-volume hydraulic conductivity testing of porous materials," in *Proceedings of the Conference on Geoenvironmental Engineering-Honoring*, pp. 69–81, Chicago, IL, USA, August 2016.

[10] D. E. Daniel, D. C. Anderson, and S. S. Boynton, "Fixed-wall versus flexible-wall permeameter," in *Hydraulic Barriers in Soil and Rock*, American Society for Testing Materials, Philadelphia, PA, USA, 1985.

[11] J. B. Franzini, "Permeameter wall effect," *Eos-Transactions American Geophysical Union*, vol. 37, no. 6, pp. 735–737, 1956.

[12] L. H. S. Roblee, R. M. Baird, and J. W. Tierney, "Radial porosity variations in packed beds," *AIChE Journal*, vol. 4, no. 4, pp. 460–464, 1958.

[13] K. Ridgway and K. J. Tarbuck, "Voidage fluctuations in randomly packed beds of spheres adjacent to a containing wall," *Chemical Engineering Science*, vol. 23, no. 9, pp. 1147–1155, 1968.

[14] C. Yoram and A. B. Metzner, "Wall effects in laminar flow of fluids through packed beds," *AIChE Journal*, vol. 27, no. 3, pp. 705–715, 1981.

[15] P. C. Carman, "Fluid flow through granular beds," *Chemical Engineering Research and Design*, vol. 75, no. 1, pp. S32–S48, 1937.

[16] A. de Klerk, "Voidage variation in packed beds at small column to particle diameter ratio," *AIChE Journal*, vol. 49, no. 8, pp. 2022–2029, 2003.

[17] K. G. Allen, T. W. von Backström, and D. G. Kröger, "Packed bed pressure drop dependence on particle shape, size distribution, packing arrangement and roughness," *Powder Technology*, vol. 246, pp. 590–600, 2013.

[18] P. K. Yadav, "Slow motion of a porous cylindrical shell in a concentric cylindrical cavity," *Meccanica*, vol. 48, no. 7, pp. 1607–1622, 2013.

[19] M. Larsson, A. Niemi, and C. F. Tsang, "A study of flow-wetted surface area in a single fracture as a function of its hydraulic conductivity distribution," *Water Resources Research*, vol. 48, no. 1, Article ID W01508, 2012.

[20] R. Kango, M. A. Alam, and V. Shankar, "Investigations of wall effect on permeability through porous media at low flow rates," *Water Science and Technology: Water Supply*, vol. 18, no. 1, pp. 233–239, 2018.

[21] D. Xie, H. Cai, and Y. Wei, "Scaling principle and method in permeability tests on coarse materials," *Chinese Journal of Geotechnical Engineering*, vol. 37, no. 2, pp. 369–373, 2015.

[22] G. D. Santa, S. Cola, M. Secco, F. Tateo, R. Sassi, and A. Galgaro, "Multiscale analysis of freeze–thaw effects induced by ground heat exchangers on permeability of silty clays," *Géotechnique*, vol. 69, no. 2, pp. 95–105, 2019.

[23] N. Moraci, M. C. Mandaglio, and I. Domenico, "A new theoretical method to evaluate the internal stability of granular soils," *Canadian Geotechnical Journal*, vol. 49, no. 1, pp. 45–58, 2012.
[24] J. Liu, *Seepage Stability and Seepage Control on Soil*, Water Resources & Electric Power Press, Beijing, China, 1992, in Chinese.
[25] L. Chen, J. Zhao, and H. Zhang, "Experimental study on suffusion of gravelly soil," *Soil Mechanics and Foundation Engineering*, vol. 52, no. 3, pp. 135–143, 2015.
[26] G. Kovacs, *Developments in Water Science*, Elsevier, Amsterdam, Netherlands, 1981.
[27] C. F. Chu and K. M. Ng, "Flow in packed tubes with a small tube to particle diameter ratio," *AIChE Journal*, vol. 35, no. 1, pp. 148–158, 1989.